Applied Catalysis B: Environmental 253 (2019) 391–400

Contents lists available at ScienceDirect

Applied Catalysis B: Environmental

journal homepage: www.elsevier.com/locate/apcatb

Peculiar kinetic properties of Cu-doped Pd/$Ce_xZr_{1-x}O_2$ in water denitrification: Impact of Pd-Cu interaction vs structural properties of $Ce_xZr_{1-x}O_2$

P. Granger[a,*], S. Troncéa[a,b], J.P. Dacquin[a,*], M. Trentesaux[a], O. Gardoll[a], N. Nuns[a], V.I. Parvulescu[b,*]

[a] Univ. Lille, CNRS, Centrale Lille, ENSCL, Univ. Artois, UMR 8181, UCCS, Unité de Catalyse et Chimie du Solide, F-59000, Lille, France
[b] University of Bucharest, Department of Organic Chemistry, Biochemistry and Catalysis, B-dul Regina Elisabeta 4-12, Bucharest, 030016, Romania

ARTICLE INFO

Keywords:
Bimetallic Pd-Cu particles
TOF-SIMS analysis
Catalytic reduction of nitrates
Drinking water

ABSTRACT

The performances of Pd-Cu bimetallic catalysts supported on ceria-zirconia were investigated in the reduction of nitrates by hydrogen. Particular attention was paid to the impact of structural heterogeneities in $Ce_xZr_{1-x}O_2$ support materials on the catalytic properties of metallic Pd and Cu nano particles. The evaporation-induced self-assembly preparation method afforded only the tetragonal structure. Co-precipitation led to a partial segregation of ceria and/or Ce-riched mixed oxide which orients differently the interactions between palladium and copper in agreement with XPS, ToF-SIMS, TEM and EDS analysis. Kinetic measurements in batch conditions led to a significant practical issue by obtaining high intrinsic rates at low Pd loading supported on $Ce_xZr_{1-x}O_2$ prepared by the self-assembly method. Ammonia as undesired by-product was usually detected. A sub-oxidation of ammonia to nitrites and nitrogen is observed with changes in the product distribution according to the preparation method of the support. Such changes have been discussed in terms intrinsic OSC properties of $Ce_xZr_{1-x}O_2$ solid solution and the stability of Pd oxidation state in the course of the reaction. An optimal Pd-Cu interaction protecting Pd to extensive oxidation was observed on highly loaded Pd-Cu on $Ce_xZr_{1-x}O_2$ prepared by the self-assembly method suggesting that ensemble effects is able to monitor the structure sensitive production of ammonia.

1. Introduction

A growing interest has been focused on innovative and scalable catalytic technologies to treat water contaminants produced from different anthropogenic sources in surface and groundwater [1–6]. This was partially motivated by the implementation of more stringent standard regulations especially toward N-containing contaminants known for generating adverse human health effects [7]. Presently, the concentration of nitrates in drinking water should not exceed 50 mg/L as set by the European legislation. This level has been significantly lowered to 10 mg/L by the U.S. Environmental Protection Agency [8]. More severe standards have been considered for permitted levels of ammonium ions with maximum concentration fixed at 0.5 mg/L [9–12]. Numerous investigations pointed out the relevance of the catalytic reduction of nitrates by hydrogen as clean reductant [13–21] compared to biological and physical treatments suffering from significant economic and ecological disadvantages due to secondary waste stream [22]. However, some critical issues were addressed to catalytic processes related to the undesired formation of ammonia and a relative low rate of nitrates reduction and/or instability. A complete suppression of ammonia was previously reported by coupling catalytic and ion exchange processes [4]. In a recent paper, we found that the use of support exhibiting oxygen storage properties can minimize the production of ammonium ions through secondary reactions [23].

Nitrate reduction to nitrogen is currently described by a two-step catalytic process according to Eqs. (1)–(3) involving the intermediate production of nitrites then sequentially reduced to nitrogen. Unfortunately, parallel reactions can also lead to undesired reaction products such as ammonium ions.

$$NO_3^- + H_2 = NO_2^- + H_2O \quad (1)$$

$$NO_2^- + 3H_2 = N_2 + 2H_2O + 2OH^- \quad (2)$$

* Corresponding authors.
E-mail addresses: pascal.granger@univ-lille.fr (P. Granger), jean-philippe.dacquin@univ-lille.fr (J.P. Dacquin), vasile.parvulescu@chimie.unibuc.ro (V.I. Parvulescu).

https://doi.org/10.1016/j.apcatb.2019.04.010
Received 17 January 2019; Received in revised form 27 March 2019; Accepted 6 April 2019
Available online 20 April 2019

Table 1
Elemental, textural analysis and reducibility of Ceria-Zirconia mixed oxides prepared through the EISA and coprecipitation method and Pd-Cu/CZ.

Sample	Ce (at. %)	Zr (at. %)	Zr /Ce	Pd (at. %)	Cu (at. %)	Pt/Cu	SSA ($m^2.g^{-1}$)	Total pore vol. ($cm^3.g^{-1}$)	Average pore size (nm)	H_2 uptake ($\mu mol.g^{-1}$) [a]
CZ(EISA)	35	65	1.86	–	–	–	98	0.10	4.5	891
CZ(COP)	43	57	1.33	–	–	–	100	0.10	6.5	1180
1Pd-0.2Cu/CZ(EISA)	41	58	1.41	0.9	0.14	6.4	n.m	n.m.	n.m.	834
1Pd-0.2Cu/CZ(COP)	28	71	2.54	0.9	0.18	5.0	n.m.	n.m.	n.m.	1100
5Pd-1Cu/CZ(EISA)	38	58	1.53	3	0.7	4.3	89	0.08	3.6	740
5Pd-1Cu/CZ(COP)	31	65	2.10	3.1	0.74	4.2	73	0.08	4.7	1140

[a] from H_2-TPR experiments.

$$NO_2^- + 3H_2 = NH_4^+ + 2OH- \quad (3)$$

Bimetallic palladium-copper particles have been found among the most efficient catalytic systems. However, more insights into the nature of reaction steps, taking place at the surface of those bimetallic particles, and the cooperative interactions between Cu, Pd and the support material are still needed in order to get more efficient catalytic systems with improved stability. Presently, the structure sensitivity on the selectivity behavior have been correctly explained on Pd particles emphasizing the key role played by copper to minimize ammonia formation but essentially on inert support materials showing that the proportion between the two metals in bimetallic ensembles can influence the selectivity towards nitrogen production [20,24]. It was also suggested that the kinetics of nitrates reduction on Pd-Cu particles could involve in some extent the support materials conventionally considered as inert in this process (as alumina for example) [25,26]. By way of illustration, Zhao et al. [25] concluded that nitrates can be first reduced on Al and Cu. Pintar et al. [25] found a Langmuir-Hinshelwood reaction mechanism taking into account non-competitive adsorptions with nitrates preferentially adsorbed on the alumina support while H_2 dissociates on supported metallic particles. In some case, the dispersion of the metallic particles on reducible supports such as TiO_2 or CeO_2 generated some spectacular changes. Indeed, more active electron-rich active metal states can be stabilized according to the strength of the metal-support interaction and induce an over hydrogenation process leading to an extra production of ammonia [21]. Epron et al. [27] pointed out the redox properties of CeO_2. These authors concluded that the nitrates reduction would occur through their interaction with oxygen vacancies. Interestingly, those authors also suggested that the successive reduction of nitrites would preferentially involve a classical Langmuir-Hinshelwood mechanism with steps taking place only on metallic Pd particles deposited on CeO_2.

The overall objective of this study was to investigate the nature of the interactions between Cu and Pd, at low and high metal loading, on the catalytic reduction of nitrates by H_2 with CeO_2-ZrO_2 mixed oxides as support material. Conventional co-precipitation and more innovative evaporation-induced self-assembly method for the preparation of CeO_2-ZrO_2 can lead to different structural and textural features [27] that could *a priori* modify the nature of the interactions with Pd and Cu. The consequences on the kinetics will be discussed in this present paper.

2. Experimental

2.1. Catalyst preparation of Pd-Cu/$Ce_xZr_{1-x}O_2$

The preparation method of $Ce_xZr_{1-x}O_2$ mixed oxides was described elsewhere [23]. Two different routes were implemented using a classical co-precipitation method by adding dropwise ammonia until pH = 10 in an aqueous solution containing the dissolved precursor salts $Ce(NO_3)_3.6H_2O$ and $ZrOCl_2{\cdot}8H_2O$. The second method combined a sol-gel route with evaporation-induced self-assembly (EISA) process in ethanol using block copolymer Pluronic P123 as template to originate a mesoporous network. A two-step drying was adopted for the oxy-hydroxide precursors obtained from the EISA method first dried at 60 °C for 24 h and then at 100 °C for another 24 h. The co-precipitated samples were dried at 120 °C for 24 h. All samples were finally calcined in air at 400 °C overnight with a temperature ramp fixed at 1 °C.min^{-1}.

The bimetallic catalysts were prepared by co-impregnation from aqueous solutions of palladium nitrate ($Pd(NO_3)_2{\cdot}2H_2O$, Sigma Aldrich) and copper nitrate ($Cu(NO_3)_2$) [24]. The co-impregnated samples were successfully dried at 100 °C overnight then calcined in air at 400 °C for 2 h and finally reduced in a flow of 60 mL.min^{-1} H_2 at 300 °C. The samples were labeled xPd-yCu/CZ(EISA) and xPd-yCu/CZ(COP) where x and y stands for the theoretical weight of palladium and copper loading equal 5 wt.% or 1 wt.% Pd and 1 wt.% or 0.2 wt.% Cu respectively. Experimental data from elemental analysis are given in atomic percentage (at.%) in Table 1. The corresponding values for the atomic Pd/Cu ratio have been also reported showing slight variation irrespective of the Pd and Cu content.

2.2. Physicochemical characterization

2.2.1. Bulk analysis

Raman spectroscopy analysis was performed on a Labram Infinity Dilor spectrometer fitted with a frequency-doubled Nd:YAG laser with an excitation radiation of 532 nm. Prior to measurements, a silicon line at 521 cm^{-1} was used for calibration. The reducibility was investigated from H_2-Temperature-Programmed Reduction (H_2-TPR) experiments on a Micromeritics Autochem II 2920 apparatus. 50 mg sample were exposed to a flow of 5 vol.% H_2 diluted in Ar (50 mL.min^{-1}) and gradually heated at a constant heating rate of 5 °C.min^{-1}. The elemental composition was measured by inductively coupled plasma-optic emission spectroscopy 720-ES ICP-OES (Agilent) with axially viewing and simultaneous CCD detection.

Transmission electron microscopy (JEOL JEM 2011) operating at 200 kV (LaB6 gun) was equipped with an energy dispersive spectroscopy (EDS) probe for analysis of the location/chemical composition of metallic particles. Before examination, samples were deposited on a molybdenum grid.

2.2.2. Surface analysis

The porosity of the catalysts samples was estimated from nitrogen physisorption measurements at −196 °C on a Micrometrics Tristar 3020 analyzer. Preliminary, the samples were cleaned after outgassing under secondary vacuum at 200 °C. The specific surface area was calculated from the BET equation and the pore volume (V_p) was estimated using the adsorption branch of the nitrogen isotherm curve.

Tof-SIMS analysis was carried out using a Tof-SIMS V instrument (ION-TOF GmbH Germany) equipped with a Bi liquid metal ion gun (LMIG). Bi_3^+ (0.3pA-25 kV) were used as primary ions for analysis in both polarities over areas of 500 µm × 500 µm. 20 scans were performed on each area with 128 × 128 pixels guaranteeing the static conditions. Charging effects due to primary ion guns were compensated with low energy electrons (20 eV). Before analysis, samples in powder form were tableted to insure a better mass resolution. We obtained a mass resolution $m/\Delta m > 4000$ at $m/z = 90$ for Zr^+ which was satisfactory for

spectroscopic investigations.

XPS spectra were recorded on an AXIS Ultra DLD Kratos spectrometer fitted with a monochromatized aluminum source for excitation (150 W). The binding energy of the C 1 s core level at 284.8 eV was used as internal reference. Semi-quantitative analysis using the integrated peak area and spectral decomposition took a Gaussian/Lorentzian peak fit into account keeping constant binding energies and peak width at half maximum as constraints.

2.3. Catalytic measurements

The reduction of nitrates by H_2 was studied at 20 °C under atmospheric pressure. 80 or 400 mg of catalyst in powder form (average grain size of 250 μm) were introduced in a 250 mL batch reactor and suspended in 40 mL of ultrapure water under a continuous flow of H_2 (200 mL/min) bubbling in the solution. 10 mL of nitrites solution (500 mg/L or 100 mg/L) were added and the suspension was stirred with a the rotation speed set at 700 rpm. Nitrates and Nitrites concentration was periodically monitored by an ionic chromatograph (Metrohm 844 UV/VIS Compact IC–Column Metrosep A Supp 16-250/4.0). The concentration of ammonium ions was measured by using an ionic chromatograph (Metrohm 861 Advanced Compact IC – column Metrosep C 6 -250/4.0).

3. Results

3.1. Impact of the structural properties of Ceria-Zirconia mixed oxide on the catalytic properties of palladium and copper in water denitrification

The influence of the metal loading on the reaction rate and product distribution was investigated in a stirred tank reactor keeping constant the atomic Pd/Cu ratio (Pd/Cu ~ 5). The initial specific rates for nitrates reduction were calculated on pre-reduced catalysts from the slopes of the tangents of the conversion curves *vs.* time at t = 0 leading to data collected in Table 2. The concentration of ammonium ions and nitrites, intermediately formed during the overall reduction process, were also plotted as a function of time. As exemplified in Figs. 1 and 2, their evolutions reflect the classical two-step reduction process earlier depicted according to Eqs. (1)–(3). We verified from preliminary experiments (not shown) that the initial rate of nitrates reduction on monometallic Pd/CZ catalyst was negligible emphasizing the fact that only copper catalyzes the first reduction step of nitrates to nitrites whereas palladium activates the subsequent reduction of nitrites [23].

3.1.1. Nitrate conversion and reaction products distribution on pre-reduced Pd-Cu/CZ

Similarly to previous investigations [23], the mass of catalysts used in catalytic testings was respectively adjusted to 80 mg or 400 mg for 5Pd-1Cu/CZ and 1Pd-0.2Cu/CZ in order to get approximately the same amount of palladium in the batch reactor. The conversion of nitrates species *vs.* time and the concentration profiles of nitrites and ammonia produced in the course of the reaction are reported in Figs. 1 and 2 for 5Pd-1Cu/CZ and 1Pd-0.2Cu/CZ respectively. As illustrated, a fast conversion of nitrates is noticeable, irrespective of the copper content, permitting their complete conversion only after 20 min. Slight changes are remarkable on Pd-Cu/CZ(COP) with a slower nitrates conversion becoming almost complete after a longer period especially on 5Pd-1Cu/CZ(COP) exceeding 50 min. Similar observations were previously reported and ascribed to an extensive copper oxidation into inactive Cu (II) species at the early stage of the reaction [28]. By comparing the initial specific rates in Table 2, superior catalytic activities are noticeable on the series Pd-Cu/CZ(EISA). According to a negligible activity of palladium to reduce nitrates, then normalized reaction rates can be calculated per copper atom taking into account the elemental analysis in Table 1 and assuming a complete accessibility, *i.e.* an atomic dispersion. Their comparison in Table 2 underlines the superior catalytic properties of 1Pd-0.2/CZ(EISA).

The nitrite concentration profiles *vs.* time described volcano-type curves currently observed which reflect the two-step reduction process as earlier described. As seen, a greater intermediate production of nitrites is usually observable on the series Pd-Cu/CZ(COP) irrespective of the Pd loading corresponding to higher concentration at maximum (see Table 2). Exceptionally, no nitrite formation was detected on 1Pd-0.2/CZ(EISA) which would suggest their fast consecutive conversion. Such an explanation seems consistent with the highest initial rate values measured on 1Pd/CZ(EISA) for the single reduction of nitrites (see Table S1 in Supplementary Information). By examining the concentration profile of ammonium ions, different regimes are observable as a function of the progress of the reaction. Indeed, a much faster production of ammonia occurs at the early stage of the reaction on 5Pd-1Cu/CZ(EISA) than on 5Pd-1Cu/CZ(COP) which could be assigned to a greater number of electron-rich active metal states as already pointed out [21] in agreement with a strengthening of the metal-support interaction. Intriguingly, 5Pd-1Cu/CZ(EISA) exhibit a peculiar kinetic behavior related to a sharp drop of ammonia concentration leading to the lowest residual concentration value after 6 h reaction, *i.e.* 187 ppm. Similar observations also characterize 5Pd-1Cu/CZ(COP) but in lower extent, the residual ammonia concentration stabilizing near 331 ppm. Such comparison underlines the occurrence of secondary reaction involving ammonia. It is worthwhile to note that the opposite trend characterize low loaded Pd and Cu catalysts. Interestingly, a successive consumption of ammonia is not observed on 1Pd-0.2Cu/CZ(EISA) whereas it occurs significantly on 1Pd-0.2Cu/CZ(COP) correlated to a stabilization of nitrites concentration and suggesting that ammonia could be re-oxidized preferentially into N_2 on the series Pd-Cu/CZ (EISA) and nitrites on Pd-Cu/CZ(COP).

3.1.2. Kinetic analysis

The kinetics of the overall reduction of nitrates has been studied in order to get more insight into the specific role played by copper and palladium and their potential interactions that could altered their intrinsic catalytic properties. As aforementioned, the overall reduction of

Table 2
Initial rate measurements for the reduction of nitrates performed at 20 °C on pre-reduced Pd-Cu/CZ.

Catalyst	Initial rate, r_0 (mol. h^{-1}.g_{Cata}^{-1})	Normalized rate r_{intr} [a]	Conc. NO_2 [b] at max (μmol.L^{-1})	Conc. NH_4^+ (μmol.L^{-1})		k_1 (min^{-1})	k_2 (min^{-1})
				max [c]	end [d]		
5Pd-1Cu/CZ(EISA)	1.76×10^{-3}	16	328	568	188	0.24	0.20
5Pd-1Cu/CZ(COP)	1.15×10^{-3}	10	492	381	331	0.06	0.12
1Pd-0.2Cu/CZ(EISA)	1.43×10^{-3}	67	~0	763	663	0.15	n.d.
1Pd-0.2Cu/CZ(COP)	0.88×10^{-3}	31	811	1329	853	0.07	0.04

[a] molec. h^{-1}.at.Cu^{-1}, calculated on the basis of the copper loading reported in Table 1.
[b] maximum concentration of nitrites intermediately formed during the sequential reduction process of nitrates.
[c] maximum concentration of ammonia formed during the reduction step of nitrites.
[d] residual ammonia concentration at the end of the reaction.

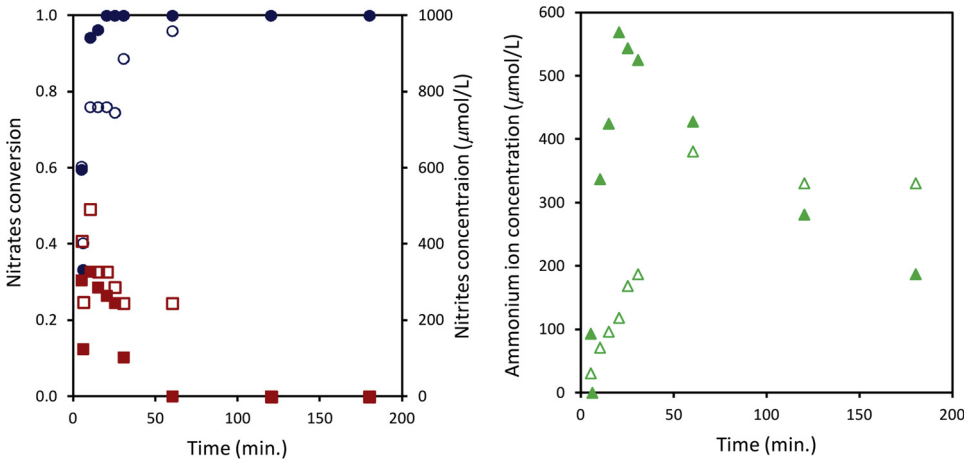

Fig. 1. Catalytic properties of 5Pd-1Cu/CZ(EISA) (full symbols) and 5Pd-1Cu/CZ(COP) (empty symbols) pre-reduced at 300 °C: Nitrate conversion (circle); Nitrites concentration (square); ammonium concentration (triangle).

nitrates can be regarded as a two-step reaction process through the production of nitrites and their subsequent consumption according to the following sequential reaction mechanism: NO_3^- NO_2^- hydrogenated products (N_2 and NH_3). In this sequence, we did not consider side reactions involving the potential re-oxidation of ammonia to nitrites and nitrogen. One can hypothesize a pseudo first order kinetics for nitrates and nitrites reduction in agreement with earlier investigations [29–31] which makes easier the resolution of the first order differential Eq. (4).

$$\frac{d[NO_2^-]t}{dt} = k_1[NO_3^-]t - k_2[NO_2^-]t \quad (4)$$

with

$$[NO_3^-]t = [NO_3^-]0\exp(-k_1 t) \quad (5)$$

The rate constant k_1 in Table 2 can be estimated from Eq. (5) by using nitrate concentration measured *vs.* time in Figs. 1 and 2. As observed the highest values still characterized the series Pd-Cu/CZ(EISA). The integration of Eq. (4) leads to Eq. (6) theoretically suited to describe the evolution of the nitrites concentration *vs.* time. A seen a maximum usually appears corresponding to a derivative almost nil which leads to (Eq. (7) and allows a rough estimation of the rate constant k_2.

$$[NO_2^-]\ t = \frac{k_1[NO_3^-]_0}{k_2 - k_1}[\exp(-k_1 t) - \exp(-k_2 t)] \quad (6)$$

$$t_{opt} = \frac{\ln k_1/k_2}{(k_1 - k_2)} \quad (7)$$

k_1 and k_2 values obtained through this method can be used as inlet values for a subsequent statistical optimization according to a classical least square method. The optimized rate constant values obtained when $\Sigma(r_{exp} - r_{cal})^2$ tends to a minimum are reported in Table 2. As seen, those kinetic parameters do not invalidate the normalized rates previously estimated but clarify the specific role of copper and palladium in the overall reduction process. It seems obvious that the values for k_1 are not sensitive to the copper loading and related changes in Cu dispersion since the reduction of nitrates is recognized as weakly structure sensitive. The lower value obtained on Pd-Cu/CZ(COP) could be equally explained by a more extensive copper oxidation which suggests weaker interactions with Pd or the support to protect the metallic character of copper.

The rate constant k_2 is expected much higher than k_1 on 1Pd-0.2Cu/CZ(EISA) because nitrites species have not been detected. On the other hand only slight difference between k_1 and k_2 are discernible for the three other samples. Based on the estimates for k_1 and k_2, predicted and experimental concentration profiles for nitrites production *vs.* time can be roughly compared in Fig. 3. As shown, an acceptable agreement is observable at the early stage of the reaction but strong divergences arise on 1Pd-0.2Cu(COP) and in a lower extent on 5Pd-1(COP) with a strong underestimation of the nitrite concentration at increasing nitrates conversion. Such a discrepancy emphasizes an extra production of nitrites through ammonia oxidation. The promotion of this reaction could

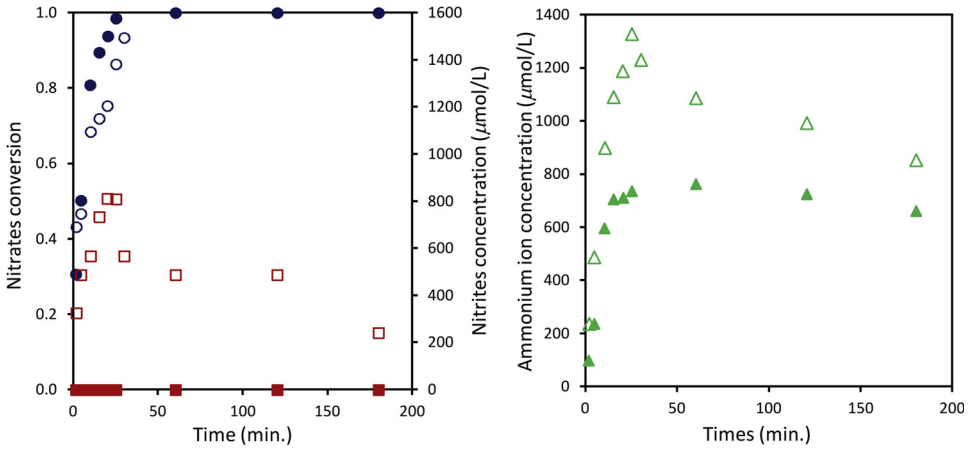

Fig. 2. Catalytic properties of 1Pd-0.2Cu/CZ(EISA) (full symbols) and 1Pd-0.2Cu/CZ(COP) (empty symbols) pre-reduced at 300 °C: Nitrate conversion (circle); Nitrites concentration (square); ammonium concentration (triangle).

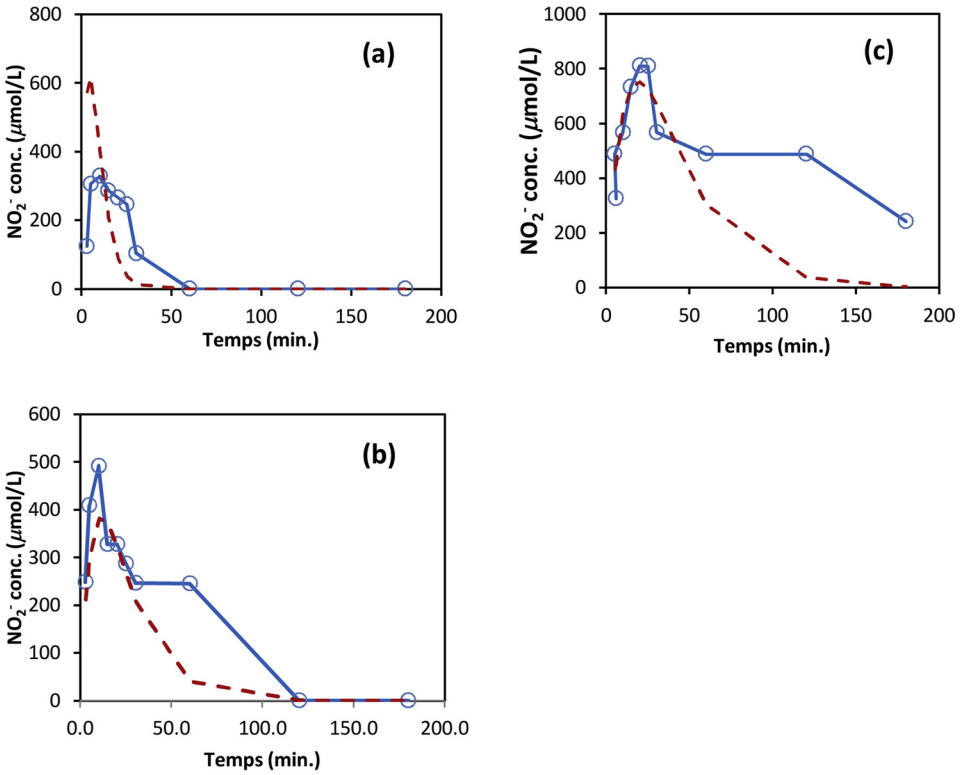

Fig. 3. Predicted and experimental nitrites concentration *vs.* time on 5Pd-1Cu(EISA) **(a)**; 5Pd-1Cu(COP) **(b)**; 1Pd-0.2Cu(COP) **(c)**.

be reasonably explained by the high ammonium ion concentration reached at the maximum but also imply the presence of an oxidizing agent. In the absence of gaseous oxygen then trace of dissolved oxygen in water and/or the lability of surface oxygen species could be involved in ad-NH_4^+ species oxidation.

3.2. Bulk and surface properties of Pd-Cu supported on Ceria-Zirconia: Impact of the preparation procedure of $Ce_xZr_{1-x}O_2$ on the nature of interaction with the metallic phase

3.2.1. Structural vs. textural properties on Ceria-Zirconia prepared through EISA or co-precipitation method

The dependence of the structural properties of Ceria-Zirconia mixed oxide on the preparation method, *i.e.* EISA *vs.* coprecipitation, was previously investigated by X-ray diffraction with reflections characterizing predominantly a tetragonal structure for CZ(EISA) solid solution whereas segregation was observed on CZ(COP) with the coexistence of a cubic phase assigned to CeO_2 or Ce-riched mixed oxide [23]. Raman spectra in Fig. 4(a), on CZ(COP), match previous XRD observations with a sharp magnification of the 490 cm^{-1} Raman line characteristic of the F2g mode for the cubic fluorite structure of CeO_2 with a space group Fm3m. Additional intense Raman lines are distinguishable on the spectrum recorded on CZ(EISA) ascribed to a tetragonal structure usually characterized by 6 Raman active modes (A1g + 2B1g + 3E2g) for the $P4_2/nmc$ space group.

Interesting comparisons were also established between structural and textural properties. Indeed, it was found that both preparation methods led essentially to the formation of mesoporous materials as exemplified in Fig. 4(b) with a stronger aggregation for CZ(COP). Nevertheless, the most prominent feature is related to changes in the narrow pore size distribution observed on CZ(EISA) becoming much broader on CZ(COP). Hence, this change in the pore size distribution could be consistent with the coexistence of a cubic CeO_2 phase or Ce-riched solid solution with the tetragonal structure of $Ce_xZr_{1-x}O_2$ for Zr-riched solid solution. The values of the specific surface area, pore volume and average pore size measured on 5Pd-1Cu/CZ(EISA) do not vary significantly. A moderate deterioration is detectable on 5Pd-1Cu/CZ(COP) which still agrees with a preferential homogeneous deposition of palladium and copper during the impregnation stage avoiding significant pore plugging on highly loaded samples after calcination.

3.2.2. TEM and EDS analysis

Ceria-zirconia grain morphologies and location of the metal particles were assessed using transmission electron microscopy equipped with an energy dispersive spectroscopy (EDS) probe for analysis of the chemical composition. TEM-EDS analyses were made on various regions of 5Pd-1Cu/CZ(COP) and 5Pd-1Cu/CZ(EISA) samples pre-reduced at 300 °C under hydrogen (see Figs. 5 and 6). First, homogeneous distribution of Ce and Zr elements constituting CZ grains is observed. However, a careful examination of 5Pd-1Cu/CZ(COP) suggests with the margin weak the presence of Ce- and Zr-riched micro domains. Pd metal particles are highlighted by the yellow spots varying between 5–50 nm in diameter. High concentration domains are observable 5Pd-1Cu/CZ(COP) which can be assigned to the result of agglomeration of larger Pd aggregates on 5Pd-1Cu/CZ(COP). With respect to palladium, copper is better dispersed irrespective of the preparation route, being present all over the support as nanoparticles with sizes estimated below 50 nm A random distribution of copper and palladium on 5Pd-1Cu/CZ (EISA) is observable (see Fig. 6) which suggests a closer interaction compared to 5Pd-1Cu/CZ(COP).

3.2.3. Impact of palladium and copper addition on the reducibility

The reducibility of bare Ceria-Zirconia samples has been earlier investigated from temperature-programmed reduction (H_2-TPR) experiments [23] confirming the existence of significant structural inhomogeneity. As shown in Fig. S1, different surface and bulk reduction processes take place ascribed to the coexistence of cubic CeO_2 (or Ce-riched $Ce_xZr_{1-x}O_2$ mixed oxide) with a tetragonal Zr-riched $Ce_xZr_{1-x}O_2$ structures on CZ(COP) [23]. These observations reflect improved oxygen mobility and related reducibility due Ce^{4+} substitution by Zr^{4+}

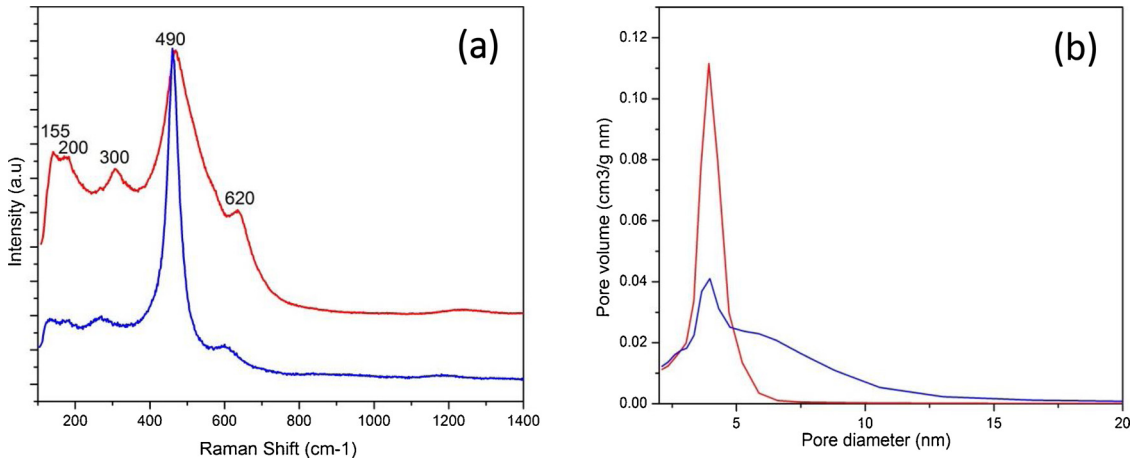

Fig. 4. (a) Raman spectra and (b) pore size distribution on CZ(EISA) (red) and CZ(COP) (blue) calcined in air at 400 °C (For interpretation of the references to colour in this figure legend, the reader is referred to the web version of this article).

[28,32,33]. As observed in Fig. S2, the addition of palladium induces a significant shift of the reduction process to much lower temperature. This improved reducibility highlights the role played by metallic palladium to activate hydrogen and facilitate a more extensive reduction of Ce^{4+} to Ce^{3+} through spill-over process [34].

Similar trends reproduce on Pd-Cu/CZ (see Fig. 7) with a sharp shift of the reduction process to lower temperature still observed. In all cases, the corresponding H_2 uptakes of $(0.72-0.73)\times10^{-3}$ mol. g^{-1} largely exceed the theoretical values expected for a complete reduction of PdO to Pd° and CuO to Cu° varying in the range $(0.09-0.34)\times10^{-3}$ mol. g^{-1} according to the metal content. High temperature signals appear in the range 350–600 °C and above 650 °C on the series Pd-Cu/CZ(COP) already discussed on bare supports and assigned to characteristic surface and bulk reduction processes of Ce^{3+} to Ce^{4+} [32–35]. Interestingly, these signals are no longer detected on Pd-Cu/CZ(EISA). Such comparison is consistent with phase segregation on CZ(COP) as reported elsewhere [23] and also suggests preferential interactions of palladium. Returning to the examination of the low temperature reduction process in Fig. 5, some changes appear associated to the formation of an asymmetric reduction peak shifting to higher temperature on Pd-Cu/CZ(COP). It is remarkable that this tendency accentuates on 1Pd-0.2Cu/CZ(COP) which could reflect weaker interactions between Pd and Cu as well as different support interactions in agreement with the existence of strong inhomogeneity on CZ(COP). Previous investigations found that highly dispersed PdO species can lose their reducibility with reduction to metallic Pd particles occurring at temperature higher than 100 °C. On the other hand, large PdO particles would reduce more readily at lower temperature T≤ 50 °C [36–38]. Copper incorporation leads to more complex phenomena because the reducibility of PdO can be alter by various types of interactions with palladium and the ceria-zirconia support. Bulk reduction of large CuO clusters usually observed above 300 °C was not detected [39] which suggests a high degree of dispersion of copper highlighted by TEM-EDS analysis. At a first glance, the formation of well-dispersed small nano-sized copper oxide particles and/or strong interactions with Ce^{4+} [40] present in Ce^{4+}–O^{2-}–Cu^{2+} structures could explain such lack of observation [41]. However, copper itself can alter the reducibility of palladium oxide species in case of strong interaction through an alloying effect.

3.2.4. XPS surface analysis of Pd-Cu/CZ

XPS measurements were performed on calcined samples. The

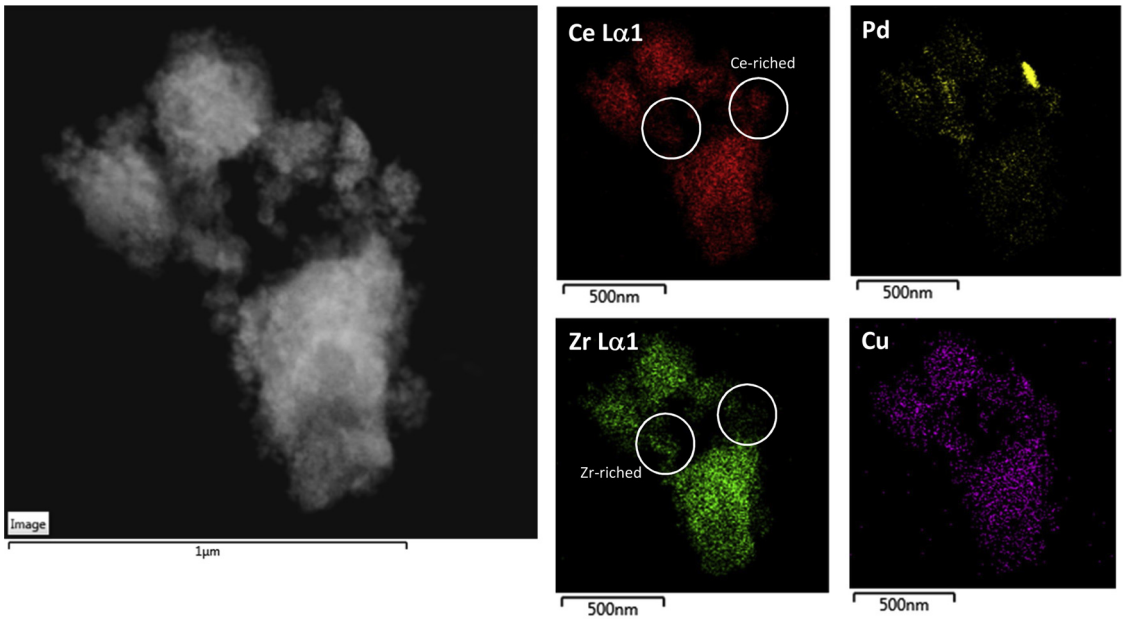

Fig. 5. TEM and EDS analysis on calcined 5Pd-1Cu/CZ(COP).

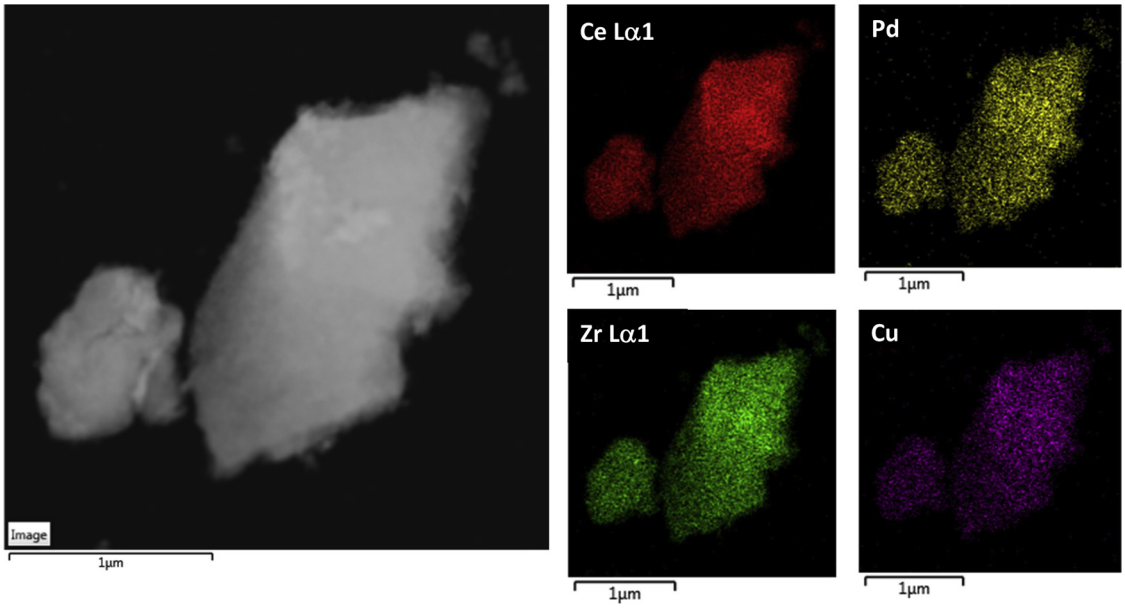

Fig. 6. TEM and EDS analysis on calcined 5Pd-1Cu/CZ(EISA).

characteristic Zr 3d, Ce 3d, O 1 s, Pd 3d and Cu 2p core levels were investigated. The binding energy values near ~182.3 eV for the Zr $3d_{5/2}$ photopeak characterize the presence of Zr^{4+}. As earlier discussed, the complexity of Ce 3d photopeak is connected to different components their decomposition giving rise to the relative concentration of Ce^{3+} and Ce^{4+} [23]. The spectral decomposition depicted in Fig. S3(a) reveal the prevalence of Ce^{4+} on calcined samples. Indeed, the estimates for the $Ce^{3+}/Ce^{3+}+Ce^{4+}$ never exceed 0.08. By comparing the B.E. value obtained on Pd $3d_{5/2}$ photopeak in the range 336.9–338.1 eV, they essentially characterize the presence of Pd^{2+} likely stabilized as PdO on calcined samples (see Table 3) excepted on 5Pd-1Cu/CZ(EISA). Indeed, the decomposition of the Pd $3d_{5/2}$ on this latter catalyst highlights two components at 337.7 eV and 339.1 eV. It is worthwhile to note that higher B.E. values did not appear on calcined 5Pd/CZ(COP). This contribution appearing near 339.1 eV has been already observed and ascribed to Pd^{4+} and/or PdO_y with $1 < y < 2$ [42–46]. In fact, different origins can explain the development of high B.E. contributions related to electron transfer monitored by the extent of interaction with the support, with copper and/or by the particle size then stabilizing the electron deficient $Pd^{\delta+}$ species with $\delta > 2$. The Cu $2p_{3/2}$ photopeak gives rise to a distinct signal only on 5Pd-1Cu/CZ(EISA) corresponding to a B.E. value of 932.7 eV. The characteristic shake up structure range 940–950 eV evidences the presence of Cu^{2+} (see Fig. S3(b) in Supplementary Information). Nevertheless, the abnormally low B.E. can suggest the coexistence of oxidic copper species stabilized in a lower oxidation state as already pointed out on bimetallic Pd-Cu systems [47,48]. At a first glance, this observation could be in connection with the appearance of the high B.E. contribution on the Pd $3d_{5/2}$ near 339.1 eV then reflecting an electron donation from Pd to Cu thanks to a closer interaction between these two elements in calcined 5Pd-1Cu/CZ(EISA). This observation could also reflect the presence of more reducible Cu(II) than on 5Pd-1Cu/CZ(COP) which would be *in situ* reduced under X-ray exposure as reported elsewhere [49]. For low loaded Pd-Cu/CZ samples, the weak intensity of the Pd 3d photopeak and a significant overlapping between Zr 3d and Pd 3d photopeaks make difficult any accurate quantitative analysis. Unfortunately, the examination of the Cu 2p core level did not lead to detectable copper species.

The examination of the surface concentration clearly indicates significant surface palladium enrichment on 5Pd-1Cu/CZ irrespective of the protocol use for the preparation of ceria-zirconia mixed oxide. Interestingly, copper is only detected on 5Pd-1Cu/CZ(EISA) which leads to a slightly lower surface atomic Pd/Cu ratio compared to elemental analysis. Such observation does not indicate significant deviation between bulk and surface composition according to the margin of

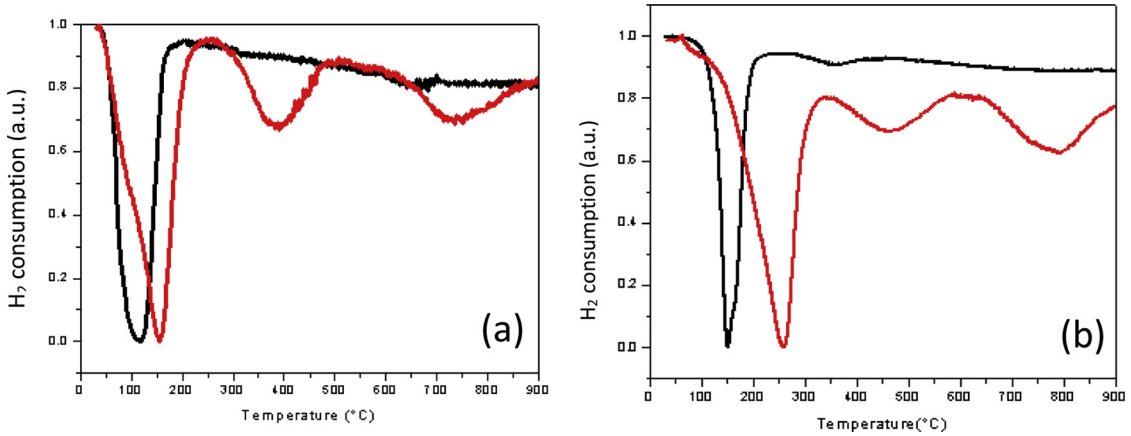

Fig. 7. H_2-TPR experiments performed on 5Pd-1Cu/CZ (a); 1Pd-0.2Cu/CZ (b) – Pd/ CZ(EISA) in black and Pd/ CZ(COP) in red (For interpretation of the references to colour in this figure legend, the reader is referred to the web version of this article).

Table 3
XPS analysis of Pd-doped Ceria-Zirconia support – Influence of the reduction temperature on the composition and oxidation state of elements.

Catalyst	Thermal Pretreatment	Binding Energy (eV)					Relative surface composition			
		Zr $3d_{5/2}$	Ce $3d_{5/2}$	O 1 s	Cu$2p_{3/2}$	Pd $3d_{5/2}$	Zr/Ce	O/Ce + Zr	Pd/Ce + Zr	Pd/Cu
5Pd/CZ(EISA)[a]	Calcined	183.0	883.7	530.4	–	338.4	1.37	2.3	0.06	
5Pd-1Cu/CZ(EISA)	Calcined	182.5	882.8	530.0	932.7	337.7/339.1	1.13 (1.53)	2.5	0.16 (0.03)	2.9 (4.3)
5Pd/CZ(COP)[a]	Calcined	182.5	883.1	530.4	–	337.3	0.93	2.7	–	
5Pd-1Cu/CZ(COP)	Calcined	182.4	883.0	530	n.d	337.3	1.35 (2.10)	3.8	0.13 (0.03)	n.d
1Pd/CZ(EISA)[a]	Calcined	182.5	883.7	530.1	–	338.1	1.80	2.2	0.07	
1Pd-0.2Cu/CZ(EISA)	Calcined	182.4	882.8	530.1	n.d	n.d.	1.04 (1.41)	2.2	- (< 0.01)	n.d
1Pd/CZ(COP)[a]	Calcined	182.6	882.7	530.1	–	337.8	0.84	2.8	0.06	
1Pd-0.2Cu/CZ(COP)	Calcined	182.1	882.0	529.5	n.d	336.9	0.48 (2.54)	2.6	0.21 (< 0.01)	n.d

The value in the bracket takes into account the elemental composition.
[a] From reference [23].

error. Useful information arises from the comparison of Zr/Ce ratio from XPS and elemental analysis. It is obvious that a sharp surface Ce enrichment occurs on the series Pd-Cu/CZ(COP) especially on 1Pd-0.2Cu/CZ(COP).

3.2.5. ToF-SIMS analysis

Time of Flight-Secondary Ion Mass Spectrometry (ToF-SIMS) can detect molecular secondary ions and then provide unique information on the coordination of elements. Hundreds of cluster ions were collected on calcined 5Pd-1Cu/CZ and spectra were particularly complex to assign due to a high number of isotopes for zirconium (5 isotopes) and palladium (6 isotopes) producing a lot of possible overlappings. In this context, a particular attention was paid to the detection of mixed oxide clusters containing Pd, Cu and O or Ce, Cu and O and their evolution on calcined and reduced samples because they reflect the close proximity of Pd and Cu in the same nano-sized aggregates. We managed to detect PdOCu cluster ions in the positive mode. Assignments were confirmed by the detection of $^{104}PdOCu^+$, $^{105}PdOCu^+$, $^{106}PdOCu^+$ and $^{108}PdOCu^+$ molecular ions in the spectra with intensities in accordance to the natural isotopic ratios. Fig. 8. reports the evolution of $PdOCu^+$ intensity on calcined and *ex situ* reduced 5Pd-1Cu/CZ(EISA) and 5Pd-1Cu/CZ(COP). A comparison can be established with the benchmark 5Pd/CZ(EISA) and 5Pd/CZ(COP). As a general trend, the contribution on mass spectra of the $PdCuO^+$ cluster ions appears more distinctly on the series 5Pd-1Cu/CZ(EISA) especially of reduced samples at 300 °C. We checked the same trend in Fig. S4 on samples reduced at 500 °C. The opposite observation is noticeable on 5Pd-1Cu/CZ(COP) while the intensity fragment is observable on the calcined sample, a strong attenuation is clearly observed in the reduced samples. This trend is also confirmed when catalyst samples are reduced at 500 °C (see Fig. S4 in supplementary Information) showing that the fragment assigned to $PdCuO^+$ cluster ions strongly attenuates on 5Pd-1Cu/CZ(COP). Among the different cluster ions identified, none of them corresponded to association between copper ceria and oxygen which could suggest a close proximity between those elements on both series. Unfortunately several attempts on low loaded catalysts, *i.e.* 1Pd-0.2Cu/CZ, did not lead to conclusive information likely due to the very low concentration of those species at the surface in agreement with XPS analysis. Hence, on the basis of those observations, one can conclude that a greater proximity would characterize Pd and Cu elements in reduced 5Pd-1Cu/CZ(EISA) samples thanks to the evolution of the intensity of $PdOCu^+$ cluster ions. This conclusion seems to be in rather agreement with TEM-EDS observations and with the evolution observed on the B.E. values measured for the Cu 2p and Pd 3d core levels.

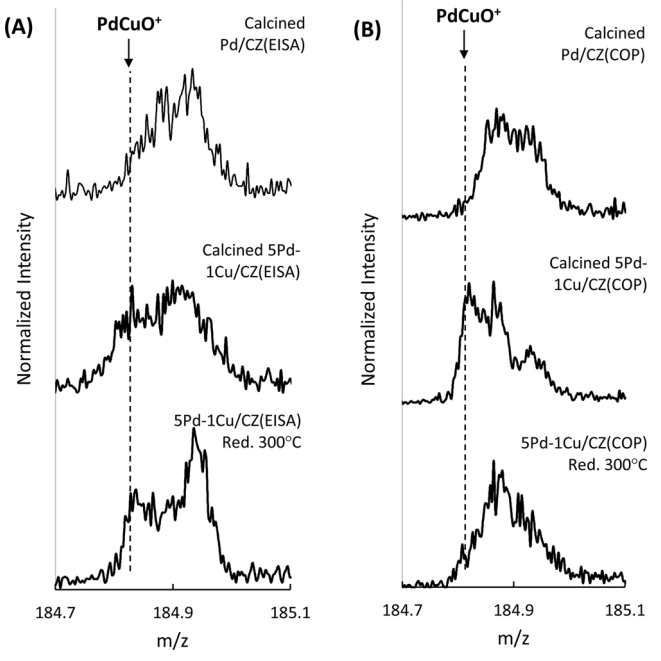

Fig. 8. *Ex situ* ToF-SIMS analysis performed on calcined and reduced bimetallic 5Pd-1Cu/CZ(EISA) **(A)** and 5Pd-1Cu/CZ(COP) **(B)**.

4. Discussion

Previous investigations reported that the reduction of nitrates on supported bimetallic Pd-Cu particles can depend on several parameters related to the metal loading, the atomic Pd to Cu ratio and the structure of ceria-zirconia supports [51]. As shown in Table 1, the values of the atomic Pd/Cu ratio slightly vary likely within the margin of error. The average Pd/Cu~5 irrespective of Pd and Cu content correspond to optimal catalytic properties in water denitrification as reported elsewhere [9]. On the other hand, we investigated the influence of the palladium loading recognized as a critical material of strategic importance by the European Union, with Pd content substantially lessened from 5 wt.% to 1 wt.%. Our kinetic measurements in batch conditions definitely show higher normalized rates of nitrates conversion on low loaded palladium catalysts, especially on 1Pd-0.2Cu/CZ(EISA). This observation is consistent with kinetic analysis leading to higher rate constant k_1 associated to the reduction of nitrates to nitrites. The lower values recorded on the series Pd-Cu/CZ(COP) could be ascribed to a greater sensibility of copper to oxidation. Another benefit associated to 1Pd-0.2Cu/CZ (EISA) is related to the lack of detection of nitrites compared to other bimetallic systems [52,53]. This behavior suggests a much faster consecutive reduction of nitrites, *i.e.* higher k_2 than on Pd-Cu/CZ(COP). Regarding the production of ammonia at the early stage of the reaction, opposite behavior characterizes Pd-Cu/CZ(EISA) and Pd-Cu/CZ(COP) catalysts, the former being more prone to produce ammonia at high Pd loading whereas the reverse trend is observable at low Pd loading. Finally the most important discrepancy in comparing predicted and experimental curves for nitrites concentration profiles is related to an

extra production over Pd-Cu/CZ(COP) which underline the occurrence of secondary reaction. All those observations underline complex surface properties depending on the degree of interaction between Pd and Cu and the peculiar properties of the support materials.

4.1. Impact of the oxidative properties of the support on the secondary ammonia oxidation

The residual concentration of ammonia at the end of the reaction (see Table 2) was found dependent on the relative rate of a secondary partial re-oxidation of ammonia to nitrites and nitrogen. As previously described, nitrogen would predominantly form on Pd-Cu/CZ(EISA) whereas a prominent production of nitrites occurs on Pd-Cu/CZ(COP) (see Fig. 3). Such observation opens the debate on the nature of the active oxygen species involved in such reaction because the nitrates reduction is performed in anaerobic conditions. Of course, one cannot strictly rule out the presence of traces of dissolved oxygen not completely degassed from water filtration which could contribute to this process. However, the more extensive re-oxidation of NH_4^+ to nitrites on 1Pd-0.2Cu/CZ(COP) and 5Pd-1Cu/CZ(COP) suggests the involvement of reactive oxygen from the support materials obeying to structural requirements. The extent of such sub-reaction likely depends on the relative surface density of those active oxygen species as well as the metal-support interface with neighbor metallic atoms capable to weaken the Ce-O bond through electron transfer. The OSC properties of ceria-based materials have been already proven in Catalytic Wet Air Oxidation [54,55]. Yang et al. evidenced the role played by the support in the activation process of oxygen on $Pt/Ce_xZr_{1-x}O_2$ [55] and demonstrated a rate enhancement in the removal of succinic acid at increasing Ce concentration. Hence, these previous observations can suggest that preferential interaction between CeO_2 or Ce-riched mixed oxide and Pd in the series Pd-Cu/CZ(COP) would be more prone to oxidize ammonia to nitrites in comparison with the series Pd-Cu/CZ(EISA). Such an explanation seems in rather good agreement with a lower surface anionic mobility of Zr-riched CZ(EISA) tetragonal structure compared to CeO_2 [56]. The evolution of Zr/Ce ratio in Table 3 with a strong surface Ce enrichment for the series Pd-Cu/CZ(COP) also agrees with this explanation. As indicated a complete explanation should also consider the oxidation state of palladium and its capability to transfer electron to weaken the Ce-O bond.

4.2. Influence of Palladium and copper loading on the extent of Pd-Cu interaction : Impact on the catalytic properties

As observed, the preservation of the metallic character of copper on Pd-Cu/CZ(COP) at the early stage of the reaction is questionable and could slower the nitrates reduction because of extensive copper oxidation. Palladium itself can suffer from surface oxidation because it currently exhibits a high oxygen affinity related to a relatively low heat of formation of metal oxide per oxygen atom then suppressing it capability to dissociate hydrogen. However, palladium in bimetallic systems can behave differently due to ligand or ensemble effects. As earlier demonstrated [57], copper can play the role of sacrificial deposit preventing surface oxidation of metallic palladium particles and preserving its capability to activate hydrogen. Subsequently electro-oxidation of hydrogen could supply the electrons needed to preserve the metallic character of copper through a concerted redox process. Based on this, the close proximity of copper and palladium in Pd-Cu/CZ(EISA) could explain the faster reduction of nitrates at the early stage of the reaction and a greater resistance to deactivation through oxidation. Until now, it was found that the peculiar properties of Pd-Cu ensembles essentially obey to structural requirements [24,28] described on large Pd crystallites which seems to be the more favorable system. In the particular case of bimetallic Pd-Cu, the close proximity of Pd and Cu atoms is also prenecessary to stabilize copper at the lowest oxidation through spill-over effect of hydrogen avoiding a complete re-oxidation of metallic copper into soluble Cu^{2+} species [51]. All those pre-requisites have been already depicted and globalized in the concept of ensemble effect where copper would govern the selectivity behavior of Pd-Cu particles through selective poisoning. Such effect would predominate on larger Pd particles expected on highly loaded Pd samples. Yoshinaga et al. [24] proposed that changes in N_2 selectivity on Pd-Cu deposited on active carbon are induced by a selective poisoning of unselective sites, *i.e.* located on the edges and corners of palladium particles at low copper loadings. On the other hand, the incorporation of high copper loading can lead by the isolation of Pd sites restoring sites for extensive production of ammonia [24]. This latter statement is of prime importance offering an explanation regarding the fast production of ammonia at the beginning of the reaction on 5Pd-1Cu/CZ(EISA). Indeed, the physicochemical characterization match properly with the formation of alloyed Pd-Cu particles where Cu and Pd would be randomly distributed. According to the surface concentration the copper surface enrichment detected would be more favorable to promote the formation of isolated Pd atoms more prone to produce ammonia instead of nitrogen. It seems also obvious that this configuration would strengthen the stability of 5Pd-1Cu/CZ(EISA) compared to 5Pd-1Cu/CZ(COP) especially if copper undetected by XPS would migrate in the support to form diffuse oxide then suppressing the Pd-Cu interaction. Except XPS there is unfortunately no strong evidence especially from ToF-SIMS analysis which reveals the presence of cationic fragment combining Cu, Ce and O.

For low palladium loading, the surface concentration of palladium is very low and the overlapping with the characteristic photopeak Zr 3d cannot lead to prominent information. Anyway the observation of the high B.E. was never observed. This seems consistent with the evolution observed on the activity and the selectivity which reflect a weak interaction between Cu and Pd preserving low coordinated Pd sites intrinsically more active towards the conversion of nitrites. H_2-TPR experiments provide useful complementary information regarding the extent of interaction between Cu and Pd because they accentuate the observations previously reported on highly loaded Pd and Cu samples. As observed on 5Pd-1Cu/CZ, an undiscernible reduction peak arises which accounts for the reaction of PdO, CuO and Ce^{4+} in $Ce_xZr_{1-x}O_2$ to Ce^{3+} whereas two reduction ranges taking place at higher temperature are observable on 5Pd-1Cu/CZ which appear more distinctly on 1Pd-0.2Cu/CZ(COP). These observations could reflect a deterioration of the Pd-Cu interface. As explained the structural inhomogeneity could play a key role on CZ(COP) associated with the coexistence of Zr-riched tetragonal $Ce_xZr_{1-x}O_2$ solid solution and the CeO_2 and/or Ce-riched mixed oxide cubic structure with preferential interaction of Pd and Cu.

5. Conclusion

A comparative study of catalytic performances of Pd-Cu/CZ catalysts in the reduction of nitrates by hydrogen shows that changes in structural properties of the support by monitoring carefully the parameters of their preparation and the metal content at constant Pd/Cu ratio influence significantly the rates of nitrates reduction and the nitrogen production. In fact, it was found that the side production of ammonia could be a tracer of the structure-sensitivity of this reaction which can be monitored by the proximity of copper and palladium. The evolution of concentration profile also reveal a secondary re-oxidation of ammonia leading preferentially to the production on nitrogen on the series Pd-Cu/CZ(EISA) and nitrites Pd-Cu/CZ(COP). The best catalytic properties were observed on low loaded Pd samples, *i.e.* on 1Pd-0.2Cu/CZ(EISA) with high reduction rate for nitrates and no detectable nitrites in solution. On the other hand, this catalyst is more prone to produce significant amount of ammonia compared to 5Pd-1Cu/CZ(EISA) which could reflect a higher stabilization of the metallic state of Pd and Cu despite higher dispersion.

The discussion on the peculiar Pd-Cu interaction was only possible on highly loaded Pd samples, the low concentration of Pd and Cu being a serious limitation on 1Pd-0.2Cu/CZ. XPS, Tof-SIMS and H_2-TPR show

that the formation of alloyed or bimetallic Pd-Cu particles would promoted on 5Pd-1Cu/CZ(EISA) protecting the metallic state of copper and palladium. TEM and EDS analysis reveals a random distribution of Cu and Pd in bimetallic particle on 5Pd-1Cu/CZ(EISA) whereas a more heterogeneous distribution with Pd islands is noticeable on 5Pd-1Cu/CZ (COP). Accordingly, the fast production of ammonia observed on 5Pd-1Cu/CZ(EISA) during the first stage of the reaction agrees with the isolation of unselective Pd sites.

For low loaded Pd and Cu samples XPS provided no strong evidence for the interaction of the two metals. This is also supported by the H_2-TPR results. The absence of the high B.E. component could be an indication of weak Pd-Cu interaction especially on 1Pd-0.2Cu/CZ(COP). Probably one cannot strictly rule out the presence of aggregates composed of Cu and Pd in close proximity. However, the faster production of ammonia at the early stage of the reaction on low loaded Pd samples could reflect a greater stabilization of electron rich Pd sites thanks to preferential strong interactions with ceria-zirconia mixed oxides.

Acknowledgments

The authors greatly acknowledge the financial support from the CCIFER – ANCS and the French Embassy (PhD fellowship awarded to S. Troncéa who won the competition *« Graine de Chercheur et Energie Durable »*). Chevreul Institute (FR 2638), Ministère de l'Enseignement Supérieur et de la Recherche, Région Nord – Pas de Calais and FEDER are acknowledged for supporting and funding partially this work. Sandra Casale (UPMC, Paris VII) is acknowledged for conducting SEM measurements.

Appendix A. Supplementary data

Supplementary material related to this article can be found, in the online version, at doi:https://doi.org/10.1016/j.apcatb.2019.04.010.

References

[1] K. Reddy, Water Res. 34 (2000) 995–1001.
[2] M. Al Bahri, L. Calvo, M.A. Gilarranz, J.J. Rodriguez, F. Epron, Appl. Catal. B 138–139 (2013) 141–148.
[3] C.P. Theologides, P.G. Savva, C.N. Costa, Appl. Catal. B 102 (2011) 54–61.
[4] Y.N. Kim, M.Y. Kim, M. Choi, Chem. Eng. J. 289 (2016) 423–432.
[5] D.P.Durkin T. Ye, J. Choi, K.J.T. Livi, H.C. De Long, P.C. Turlove, D.H. Fairbrother, L.M. Haverhals, D. Shuai, Appl. Catal. B 221 (2018) 290–301.
[6] M. Pera-Titus, M. Fridmann, N. Guilhaume, K. Fiaty, J. Membr. Sci. 401–402 (2012) 204–216.
[7] L.J. Puckert, Environ. Sci. Technol. 29 (1995) 408A–414A.
[8] U.S. Environmental Protection Agency, USEPA, 2008 Title 40, Part 141.54:425.
[9] S. Hörold, K.D. Vorlo, T. Tacke, M. Sell, Catal. Today 17 (1993) 21–30.
[10] A. Suda, H. Sobukawa, T. Suzuki, T. Kandori, Y. Ukyo, M. Sugiura, J. Ceram. Soc. Jpn. 109 (2001) 177–180.
[11] S. Letichevsky, C.A. Tellez, R.R. de Avillez, M.I.P. da Silva, M.A. Fraga MA, L.G. Appel, Appl. Catal B: Environ. 58 (2005) 203–210.
[12] A.I. Kozlov, D.H. Kim, A. Yezerets, P. Andersen, H.H. Kung, M.C. Kung, J. Catal. 209 (2002) 417–426.
[13] F. Epron, F. Gauthard, C. Pineda, J. Barbier, J. Catal. 198 (2001) 309–318.
[14] M.-S. Kim, D.-W. Lee, S.H. Chung, J.T. Kim, I.-H. Cho, K.-Y. Lee, J. Mol. Catal. A 392 (2014) 308–314.
[15] J. Kugai, J.T. Miller, N. Guo, C. Song, Appl. Catal B: Environ. 105 (2011) 306–316.
[16] M.-S. Kim, S.-H. Chung, C.J. Yoo, M.S. Lee, I.-H. Cho, D.-W. Lee, K.-Y. Lee, Appl . Catal. B 142–143 (2013) 354–361.
[17] M.-S. Kim, S.-H. Chung, C.J. Yoo, M.S. Lee, I.-H. Cho, D.-W. Lee, K.-Y. Lee, Appl. Catal. B 142–143 (2013) 354–361.
[18] M. Al Bahri, L. Calvo, M.A. Gilarranz, J.J. Rodriguez, F. Epron, Appl. Catal. B 138–139 (2013) 141–148.
[19] F. Deganello, L.F. Liotta, A. Macaluso, A.M. Venezia, G. Deganello, Appl. Catal. B 24 (2000) 265–273.
[20] U. Prüsse, K.D. Vorlop, J. Mol. Catal. 173 (2001) 313–328.
[21] N. Barrabés, A. Dafinov, F. Medina, J.E. Sueiras, Catal. Today 149 (2010) 341–347.
[22] M.G. Davie, H. Cheng, G.D. Hopkins, C.A. Lebron, M. Reinhard, Environ. Sci. Technol. 42 (2008) 8908–8915.
[23] P. Granger, S. Troncéa, J.P. Dacquin, M. Trentesaux, V.I. Parvulescu, Appl. Catal. B 224 (2018) 648–659.
[24] Y. Yoshinaga, T. Akita, I. Mikami, T. Okura, J. Catal. 207 (2002) 37–45.
[25] W. Zhao, X. Zhu, Y. Wang, Z. Ai, D. Zhao, Chem. Eng. J. 254 (2014) 410–417.
[26] A. Pintar, J. Batista, J. Levec, T. Kajiuchi, Appl. Catal. B 11 (1996) 81–98.
[27] F. Epron, F. Gauthard, J. Barbier, J. Catal. 206 (2002) 363–367.
[28] J. Sá, H. Vinek, Appl. Catal. B 57 (2005) 247–256.
[29] A.M.E. Khalil, O. Eljamal, S. Jribi, N. Matsunaga, Chem. Eng. J. 287 (2016) 367–380.
[30] G.C.C. Yang, H.L. Lee, Water Res. 39 (2005) 884–894.
[31] Z. Zhang, Z. Hao, Y. Yang, J. Zhang, Q. Wang, X. Xu, Desalination 257 (2010) 158–162.
[32] F.B. Passos, E.R. de Oliveira, L.V. Mattos, F.B. Noronha, Catal. Today 101 (2005) 23–30.
[33] P. Fornasiero, G. Balducci, R. Di Monte, J. Kaspār, V. Sergo, G. Gubitosa, A. Ferrero, M. Graziani, J. Catal. 164 (1996) 173–183.
[34] N. Hickey, P. Fornasiero, J. Kaspar, J.M. Gatica, S. Bernal, J. Catal. 200 (2001) 181–193.
[35] C. Bozo, N. Guilhaume, E. Garbowski, M. Primet, Catal. Today 59 (2000) 33–45.
[36] H. Muraki, K. Yokota, Y. Fujitani, Appl. CataI. 48 (1989) 93–105.
[37] G. Chen, W.-T. Chou, C.-T. Yeh, Appl. Catal. 8 (1983) 389–397.
[38] I. Halasz, A. Brenner, M. Shelef, K.Y.S. Ng, Appl. Catal. A 82 (1992) 51–63.
[39] Javier Giménez-Mañogil, Avelina García-García, Appl. Catal. A 542 (2017) 226–237.
[40] M. Luo, J. Ma, J. Lu, Y. Song, Y. Wang, J. Catal. 246 (2007) 52–59.
[41] Q. Liang, X. Wu, D. Weng, Z. Lu, Catal. Commun. 9 (2008) 202–206.
[42] W. Huang, Z. Zuo, P. Han, Z. Li, T. zhao, J. Electron Spectrosc. Relat. Phenom. 173 (2009) 88–95.
[43] E.M. Slavinskaya, O.A. Stonkus, R.V. Gulyaev, A.S. Ivanova, V.I. Zaikovskii, P.A. Kuznetsov, A.I. Boronin, Appl. Catal. A 401 (2011) 83–97.
[44] K. Otto, L.P. Haack, J.E. de Vries, Appl. Catal. B 1 (1992) 1–12.
[45] M. Moroseac, T. Skála, K. Veltruská, V. Matolín, I. Matolínová, Surf. Sci. 56 (2004) 1118–1123.
[46] P. Miquel, Y. Yamin, K. Lombaert, C. Dujardin, M. Trenteseaux, L. Gengembre, P. Granger, Surf. Interface Anal. 42 (2010) 545–550.
[47] D. Das, J. Llorca, M. Dominguez, S. Colussi, A. Trovarelli, A. Gayen, Int. J. Hydrogen Energy 40 (2015) 10463–10479.
[48] M. Hronec, K. Fulajtárová, I. Vávra, T. Soták, E. Dobročka, Appl. Catal. B 181 (2016) 210–219.
[49] A. Schön A, J.P. Dacquin, P. Granger, C. Dujardin, Appl. Catal. B 223 (2018) 167–176.
[51] W. Gao, N. Guan, J. Chen, X. Guan, R. Jin, H. Zheng, Z. Liu, F. Zhang, Appl. Catal. B 46 (2003) 341–351.
[52] O.S.G.P. Soares, J.J.M. Órfão, M. F.R. P. Desalin. 279 (2011) 367–374.
[53] A. Devadasa, S. Vasudevanb, F. Epron, J. Hazard. Mater. 185 (2011) 1412–1417.
[54] S. Keav, A. Espinoza de los Monteros, J. Barbier Jr., D. Duprez, Appl. Catal. B 150-151 (2014) 402–410.
[55] S. Yang, M. Besson, C. Descormes, Appl. Catal. B 100 (2010) 282–288.
[56] S.A. Ghom, C.Z. Zamani, S. Nazarpour, T. Andreu, J.R. Morante, Sens. Actuators B 140 (2009) 216–221.
[57] J. Barbier, J.M. Dumas, C. Géron, H. Hadrane, Appl. Catal. 67 (1990) L1–L4.

Further reading

[50] F. Amano, T. Tanaka, T. Funabiki, J. Mol. Catal. A 221 (2004) 89–95.